Biomedicine & Pharmacotherapy 156 (2022) 113896

Contents lists available at ScienceDirect

Biomedicine & Pharmacotherapy

journal homepage: www.elsevier.com/locate/biopha

The *ADORA1* mutation linked to early-onset Parkinson's disease alters adenosine A_1-A_{2A} receptor heteromer formation and function

Laura I. Sarasola [a,b,1], Claudia Llinas del Torrent [c,1], Andrea Pérez-Arévalo [a,b], Josep Argerich [a,b], Nil Casajuana-Martín [c], Andy Chevigné [d], Víctor Fernández-Dueñas [a,b], Sergi Ferré [e,*], Leonardo Pardo [c,*], Francisco Ciruela [a,b,**]

[a] Pharmacology Unit, Department of Pathology and Experimental Therapeutics, School of Medicine and Health Sciences, Institute of Neurosciences, University of Barcelona, 08907 L'Hospitalet de Llobregat, Spain
[b] Neuropharmacology & Pain Group, Neuroscience Program, Bellvitge Institute for Biomedical Research, 08907 L'Hospitalet de Llobregat, Spain
[c] Laboratory of Computational Medicine, Biostatistics Unit, Faculty of Medicine, Universitat Autònoma Barcelona, Bellaterra, 08193 Barcelona, Spain
[d] Immuno-Pharmacology and Interactomics, Department of Infection and Immunity, Luxembourg Institute of Health (LIH), Esch-sur-Alzette, Luxembourg
[e] Integrative Neurobiology Section, National Institute on Drug Abuse, Intramural Research Program, National Institutes of Health, Baltimore, MD, USA

ARTICLE INFO

Keywords:
Adenosine A_1 receptor
Early-onset Parkinson's disease
A_1R-A_{2A}R heteromer
Constitutive activity

ABSTRACT

Adenosine modulates neurotransmission through inhibitory adenosine A_1 receptors (A_1Rs) and stimulatory A_{2A} receptors (A_{2A}Rs). These G protein-coupled receptors are involved in motor function and related to neurodegenerative diseases such as Parkinson's disease (PD). An autosomal-recessive mutation (G279$^{7.44}$S) within the transmembrane helix (TM) 7 of A_1R (A_1R^{G279S}) has been associated with the development of early onset PD (EOPD). Here, we aimed at investigating the impact of this mutation on the structure and function of the A_1R and the A_1R-A_{2A}R heteromer. Our results revealed that the G279$^{7.44}$S mutation does not alter A_1R expression, ligand binding, constitutive activity or coupling to transducer proteins ($G_{\alpha i}$, $G_{\alpha q}$, $G_{\alpha 12/13}$, $G_{\alpha s}$, β-arrestin2 and GRK2) in transfected HEK-293 T cells. However, A_1R^{G279S} weakened the ability of A_1R to heteromerize with A_{2A}R, as shown in a NanoBiT assay, which led to the disappearance of the heteromerization-dependent negative allosteric modulation that A_1R imposes on the constitutive activity and agonist-induced activation of the A_{2A}R. Molecular dynamic simulations allowed to propose an indirect mechanism by which the G279$^{7.44}$S mutation in TM 7 of A_1R weakens the TM 5/6 interface of the A_1R-A_{2A}R heteromer. Therefore, it is demonstrated that a PD linked *ADORA1* mutation is associated with dysfunction of adenosine receptor heteromerization. We postulate that a hyperglutamatergic state secondary to increased constitutive activity and sensitivity to adenosine of A_{2A}R not forming heteromers with A_1R could represent a main pathogenetic mechanism of the EOPD associated with the G279$^{7.44}$S *ADORA1* mutation.

1. Introduction

Parkinson's disease (PD), the second-most common neurodegenerative disease after Alzheimer's disease, is a movement disorder characterized by motor dysfunction, presence of intracellular inclusions containing aggregates of α-synuclein (i.e., Lewy bodies) and neuronal loss within the substantia nigra causing dopamine deficiency [1,2]. It affects 2–3% of the population above 65 years of age [2,3] and the mean age of onset is within the early 60 s [4]. Early-onset PD (EOPD), which accounts for 5–10% of all PD cases, is defined as the onset of parkinsonism before age 40 (occasionally 50) [5]. Although usually idiopathic, up to 5–10% of PD cases are believed to be associated to heritable genetic factors [1,3], and there is some evidence indicating that EOPD is often dependent on autosomal-recessive inheritance of certain genes [6]. In EOPD, the progression of parkinsonism is slower and the response to dopaminergic agents is often effective [7].

* Corresponding authors.
** Corresponding author at: Pharmacology Unit, Department of Pathology and Experimental Therapeutics, School of Medicine and Health Sciences, Institute of Neurosciences, University of Barcelona, 08907 L'Hospitalet de Llobregat, Spain.
E-mail addresses: sferre@intra.nida.nih.gov (S. Ferré), Leonardo.Pardo@uab.es (L. Pardo), fciruela@ub.edu (F. Ciruela).
[1] Contributed equally to this work

https://doi.org/10.1016/j.biopha.2022.113896
Received 19 July 2022; Received in revised form 17 October 2022; Accepted 17 October 2022
Available online 21 October 2022

PD management is based on dopamine replacement pharmacotherapies with L-DOPA being the gold standard drug, usually in the presence of catechol-O-methyltransferase and/or monoamine oxidase type B inhibitors [2]. However, log-term treatment with L-DOPA leads almost invariably to motor complications [2]. Since dopamine acts on striatal medium spiny neurons through dopamine D_1 and D_2 receptors (D_1Rs and D_2Rs, respectively), agonists at these receptors (mainly at D_2Rs) are also commonly used in PD [8]. Moreover, non-dopaminergic agents targeting other pharmacological systems are also being interrogated to avoid L-DOPA therapy complications [9]. In fact, adenosine A_{2A} receptor (A_{2A}R) antagonists have emerged as complementary non-dopaminergic drugs to alleviate PD [10]. The US Food and Drug Administration (FDA) recently approved the A_{2A}R antagonist istradefylline (Nourianz®; developed by Kyowa Hakko Kirin Inc., Japan), as an add-on treatment to L-DOPA in PD with "OFF" episodes [11]. A_{2A}R blockade favours D_2R signalling through allosteric interactions in the A_{2A}R-D_2R heteromer localized in the striatal GABAergic efferent neurons that project to the pallidal complex, the striatopallidal neurons [12,13]. Together with the ability of A_{2A}R to control the corticostriatal terminal release of glutamate, striatal A_{2A}Rs provide a strong molecular substrate that harmonizes dopaminergic and glutamatergic transmission in health and disease (i.e., PD) [12], thus justifying targeting A_{2A}R signalling in PD.

Adenosine A_1 receptors (A_1Rs) show a widespread distribution in the brain, with their highest density detected in the cortex, hippocampus, cerebellum, and basal ganglia [14]. Within the striatum, A_1Rs are expressed by the GABAergic efferent neurons, the cortical glutamatergic afferent terminals, and by the dopaminergic projections from the mesencephalon [15,16], thus tuning the striatal circuitry and motor function [17]. Consequently, A_1R may play a key role in the dopaminergic and glutamatergic dysregulation observed in PD [18,19]. A complex array of presynaptic receptors, including the dopamine receptor subtypes D_2R and dopamine D_4 receptor (D_4R), the adenosine receptor subtypes A_1R and A_{2A}R and cannabinoid CB_1 receptors (CB_1Rs), are located at the corticostriatal terminals and regulate glutamate release in the striatum [20–24]. Therefore, dysregulation of these presynaptic modulatory receptors can lead to abnormal glutamate release leading to disorders that affect brain circuits involved in motor function control [18,23]. Importantly, A_1R and A_{2A}R form heteromers in the presynaptic membrane of corticostriatal glutamatergic synapses, where they seem to act as an adenosine concentration-dependent switch, by which low and high adenosine concentrations inhibit and stimulate, respectively, glutamate release [20,25].

Genetic analysis (including genome-wide single-nucleotide polymorphism homozygosity mapping and exome sequencing) identified an autosomal-recessive mutation ($G279^{7.44}S$) within the A_1R gene (*ADORA1*) as a probable cause of EOPD in two brothers from an Iranian family [26]. Although some functional consequences of this mutation have recently been proposed [27], there is some controversy about *ADORA1* as a candidate gene in PD [28,29]. Here, we evaluated the impact of the $G279^{7.44}S$ A_1R gene mutation on receptor expression and function and on its ability to heteromerize with A_{2A}R, upon heterologous expression in HEK-293 T cells. Specifically, the $G279^{7.44}S$ A_1R gene mutation led to a decrease in A_1R-A_{2A}R heteromerization, with the consequent withdrawal of the negative allosteric influence of the A_1R on A_{2A}R function.

2. Materials and methods

2.1. Reagents

The ligands used were CA200634 (Hello Bio; County Meath, Republic of Ireland), 8-cyclopentyl-1,3-dipropylxanthine (DPCPX; Tocris Bioscience, Bristol, United Kingdom), N6-cyclopentyladenosine (CPA; Tocris Bioscience), CGS21680 (Tocris Bioscience) and SCH442416 (Tocris Bioscience). The antibodies used were mouse anti-HA (sc-7392, Santa Cruz Biotechnology Inc., Dallas, TX, USA), rabbit anti-A_1R (sc-28995, Santa Cruz Biotechnology Inc.), rabbit anti-α-actinin (sc-17829; Santa Cruz Biotechnology Inc.), HRP-conjugated goat anti-rabbit IgG (Pierce Biotechnology, Rockford, IL, USA) and Cy3-conjugated donkey anti-mouse antibody (Jackson Immunoresearch Laboratories Inc., West Grove, PA, USA). Other reagents used were Dulbecco's modified Eagle's medium (DMEM) (Sigma Aldrich, St. Louis, MO, USA), coelenterazine 400a (NanoLight Technologies; Pinetop, AZ, USA) and adenosine deaminase (ADA; Diagnostics Roche, Indianapolis, IN, USA).

2.2. Plasmids

The human A_1R cloned in pNLF1-secN (Promega, Madison, WI, USA) was mutated (835 G>A) using the QuickChange II kit (Agilent Technologies, Santa Clara, CA, USA) and the forward (5'-CATGGCCGAGTTGCTGTGCGTGAGGAAGA-3') and reverse (5'-TCTTCCTCACGCACAGCAACTCGGCCATG-3') primers (Biomers, Ulm, Germany) following the manufacturer recommendations. The mutation was verified by DNA sequencing. A pIREShyg3 and pIRESneo3 (Clontech Laboratories, Mountain View, CA, USA) containing the signal peptide (SP) of the human metabotropic glutamate receptor type 5, the hemagglutinin (HA)-epitope tag and the NanoLuc luciferase (NL) at the 5' of the multicloning site (MCS) of the vector were generated (GenScript Biotech, Leiden, The Netherlands). Subsequently, human A_1R^{wt} and A_1R^{G279S} were cloned in frame into pIREShyg3-SP-HA-NL between *Age*I and *Eco*RI restriction enzyme sites to generate the A_1R^{wt}-NL and A_1R^{G279S}-NL constructs, thus containing the SP, HA, and NL at the N-terminus of the receptor. In addition, A_1R^{wt} and A_1R^{G279S} were cloned in frame into pIREShyg3 containing the sequence encoding LgBiT or SmBiT of NL (Promega) at the 3'of the MCS. Thus, the cDNA encoding A_1R^{wt} and A_1R^{G279S} was amplified by PCR using the primers FXho (5'-CAGCG**CTCGAG**CCGCCCTCCATCTCAGCTTTCC-3') and RNot (5'-ACAGCG**GCGGCCGC**GTCATCAGGCCTCTCTCTTCTGGG-3') and cloned into the *Xho*I/*Not*I restriction enzyme sites of pIREShyg3-SmBit or pIREShyg3-LgBiT plasmids. Also, the cDNA encoding the human A_{2A}R was amplified using the primers FBam (5'- CGT**GGATCC**CCCATCATGGGCTCCTCGGTGTACATCACG-3') and R*Eco*RV (5'- AAACAC**GATATC**GGACACYCCYGCAGGYAGGACCCG-3'). and cloned into *Bam*HI/*Eco*RV restriction enzyme sites of pIREShyg3-LgBiT.

The plasmids encoding the mini-Gαi, mini-Gαs, mini-Gαq and mini-Gα12/13 proteins (engineered GTPase domain of Gα subunit) linked to the LgBiT were previously described [30–32]. Similarly, the plasmids encoding the β-arrestin2 and GRK2-LgBiT were kindly provided by Dr. K. Sahlholm (Karolinska Institute, Stockholm, Sweden). All transduction proteins were cloned into a pNBe3 vector (Promega) and verified by sequencing.

2.3. Cell culture and transfection

Human embryonic kidney (HEK)− 293 T cells obtained from ATCC (CRL-321, RRID:CVCL_0063) were grown in DMEM supplemented with 1 mM sodium pyruvate (Biowest, Nuaillé, France), 2 mM L-glutamine (Biowest), 100 U/ml streptomycin (Biowest), 100 mg/ml penicillin (Biowest) and 5% (v/v) foetal bovine serum (Invitrogen). Manipulation and maintenance were carried out in a biological safety cabinet Class 1 and in an incubator at 37 °C, 5% CO_2 and 90% relative humidity. HEK-293 T cells stably expressing A_1R^{wt}-NL, A_1R^{G279S}-NL or A_{2A}R-NL were grown in the presence of geneticin (1 mg/ml, Santa Cruz Biotechnology, Dallas, USA). Finally, HEK-293 T cells were transiently transfected with the indicated cDNA construct using polyethylenimine (PEI, 1 mg/ml, Sigma Aldrich), as previously described [33].

2.4. Immunocytochemistry

HEK-293 T cells stably expressing A_1R^{wt}-NL and A_1R^{G279S}-NL were grown on poly-D-lysine (0.1 mg/ml) coverslips, fixed in 4%

paraformaldehyde for 15 min and washed with PBS containing 20 mM glycine (buffer A) to quench aldehyde groups. Cells were then permeabilized with buffer A containing 0.2% Triton X-100 for 10 min. Subsequently, cells were blocked with 10% BSA labelled overnight at 4 °C with a mouse anti-HA, washed, and stained with Cy3-conjugated donkey anti-mouse IgG antibody (1:200). Coverslips were rinsed for 3 min in PBS, mounted with Vectashield immunofluorescence medium (Vector Laboratories, Peterborough, UK) containing DAPI and examined using a Leica TCS 4D confocal scanning laser microscope (Leica Lasertechnik GmbH, Heidelberg, Germany).

2.5. Biotinyilation assay, gel electrophoresis, and immunoblotting

Biotinylation of cell surface proteins was performed as previously described [34]. Briefly, HEK-293 T cells stably expressing A_1R^{wt}-NL and A_1R^{G279S}-NL were treated with EZ-Link™ NHS-Biotin (50 μg/μl; ThermoFisher, Waltham, MA, USA) before membrane extracts were obtained by mechanical homogenization and centrifugation (16000 x g, 30 min). Membrane extracts were solubilized in 1 ml of ice-cold radioimmunoassay (RIPA) buffer (100 mM NaCl, 1% TritonX-100, 50 mM Tris-HCl, 0.5% sodium deoxycholate, 1 mM EDTA, and 0.2% SDS, pH 7.5) for 30 min on ice before centrifugation (16000 x g, 30 min). Solubilized membrane extract (900 μl) was incubated with streptavidin-conjugated agarose (Sigma Aldrich) in constant rotation (300 rpm) at 4 °C overnight. The remaining (100 μl) solubilized membrane extract was precipitated with acetone at − 20 °C overnight. Both the biotinylatedcell surface and total protein extracts were analysed by sodium dodecyl sulphate–polyacrylamide gel electrophoresis (SDS/PAGE) using 10% polyacrylamide gels. Separated proteins were transferred to polyvinylidene difluoride (PVDF) membranes using a semi-dry transfer system (Bio-Rad, Hercules, CA, USA), immunoblotted with the indicated antibody and then with the horseradish peroxidase (HRP)-conjugated corresponding secondary antibody. The immunoreactive bands were developed using a chemiluminescent detection kit (Thermo Fisher Scientific, Waltham, MA, USA) and detected with an Amersham Imager 600 (GE Healthcare Europe GmbH, Barcelona, Spain) [35].

2.6. NanoBRET experiments

The NanoBRET assay was performed on cells expressing A_1R^{wt}-NL and A_1R^{G279S}-N as previously described [36]. In brief, cells were re-suspended in Hank's Balanced Salt Solution (HBSS; 137 mM NaCl, 5.4 mM KCl, 0.25 mM Na_2HPO_4, 0.44 mM KH_2PO_4, 1.3 mM $CaCl_2$, 1.0 mM $MgSO_4$, 4.2 mM $NaHCO_3$, pH 7.4) containing ADA (0.5 U/ml) and plated into poli-ornitine coated white 96-well plates. After 24 h, cells were challenged with the fluorescent A_1R antagonist (CA200634) in the presence or absence of DPCPX and incubated for 1 h at 37 °C. Subsequently, coelenterazine 400a was added at a final concentration of 1 μM, and readings were performed after 5 min using a CLARIOStar plate reader (BMG Labtech; Durham, NC, USA). The donor and acceptor emission were measured at 490 ± 10 nm and 650 ± 40 nm, respectively. The raw NanoBRET ratio was calculated by dividing the 650 nm emission by the 490 nm emission and the values fitted by nonlinear regression using GraphPad Prism 9 (GraphPad Software, La Jolla, CA, USA). The results were expressed as a percentage of the maximum signal obtained (mBU; miliBRET units).

2.7. NanoBiT assay

The NanoBiT assay was performed as previously described [37]. HEK-293 T cells transiently transfected with A_1R^{wt}-SmBiT or A_1R^{G279S}-SmBiT plus $G_{i/o}$-LgBiT, G_q-LgBiT, $G_{12/13}$-LgBiT, G_s-LgBiT, β-arrestin2-LgBiT or GRK2-LgBiT were harvested in Opti-MEM (ThermoFisher, Waltham, MA, USA) containing ADA (0.5 U/ml), transferred (90 μl) into a white 96 well plate (Corning™ 96-Well, Cell Culture-Treated, Flat-Bottom microplate; 50,000 cells/cm^2) and incubated for 1 h at 37 °C. Subsequently, 10 μl of a 10 μM coelenterazine 400a solution was added to each well. After one-minute incubation end-point luminescence was determined using a CLARIOstar plate-reader, and the output luminescence was reported as the integrated relative light units (RLU). Immediately after basal measurement agonist/antagonists were added and luminescent signal was measured every 5 min for 1 h. The luminescence signal (RLU) was normalized as indicated:

$$\frac{RLU_{sample} - RLU_{basal}}{RLU_{basal}}$$

2.8. cAMP accumulation

HEK-293 T cells stably expressing $A_{2A}R$-NL were transiently transfected with A_1R^{wt}-NL, A_1R^{G279S}-NL or empty vector and the intracellular cAMP accumulation was measured using the LANCE Ultra cAMP kit (PerkinElmer, Waltham, MA, USA) as previously described [38]. Briefly, cells (8×10^5 cells/200 μl) were incubated with stimulation buffer consisting of DMEM containing 0.1% BSA, ADA (0.5 U/ml), and the zardaverine (100 μM) for 1 h at 37 °C in constant rotation (300 rpm). The cells were then incubated with CGS21680 in stimulation buffer containing at 37 °C for 30 min. Subsequently, 10 μl of cells were seeded in a 384-well plate and ULight anti-cAMP antibody and Eu-cAMP tracer were added according to the manufacturer's indications. TR-FRET was quantified in a POLARStar microplate reader (BMG Labtech). Only data suited to the standard range were used for analysis.

2.9. Computational methods

The inactive structure of A_1R (PDB id 5UEN) [39] and $A_{2A}R$ (5IU4) [40] was used. Fusion proteins were removed, and stabilizing mutations were mutated to the native sequence. Internal water molecules observed in the high-resolution structure of $A_{2A}R$ were incorporated in both A_1R and $A_{2A}R$ models. $S279^{7.44}$ in A_1R^{G279S} was modelled in both rotameric *g*- and *g*+ states. The A_1R-$A_{2A}R$ heteromer was built from the TM 5/6 dimeric interface observed in the crystal structure of μ-opioid receptor (4DKL) [41], as previously performed [42]. A_1R^{wt}, A_1R^{G279S}, A_1R^{wt}-$A_{2A}R$, and A_1R^{G279S}-$A_{2A}R$ were embedded in a lipid bilayer box, constructed using PACKMOL-memgen [43], containing 1-palmitoyl-2-oleoyl-sn-glycero-3-phosphocholine, water molecules, and monoatomic Na^+ and Cl^- ions. MD simulation of these systems was performed with GROMACS 2019 [44] using the previously reported protocol [45]. Trajectories analysis was performed using MDAnalysis [46]. In particular, we used unit twist angle to measure local helix uniformity. This parameter is calculated for sets of four consecutive Cα atoms, and it is interpreted as follows: an ideal α-helix, with approximately 3.6 residues per turn, has a twist angle of approximately 100º (360/3.6); a closed helix segment, with < 3.6 residues per turn, possesses a twist $> 100º$, whereas an open helix segment, with > 3.6 residues per turn, possesses a twist $< 100º$.

2.10. Statistics

Data are represented as mean ± standard error of mean (SEM) with statistical significance set at $P < 0.05$. The number of samples (n) in each experimental condition is indicated in the legend of the corresponding figure. Outliers were assessed using the ROUT method [47], thus no sample was excluded assuming a Q value of 1% in GraphPad Prism 9. Comparisons between experimental groups were performed using Student's *t* test, one- or two-way factor analysis of variance (ANOVA) followed by Tukey's multiple comparisons *post-hoc* test and comparisons between curve fits were performed using the extra sum-of-squares F test using GraphPad Prism 9 as indicated.

3. Results

3.1. Heterologous expression of the G279$^{7.44}$S mutation in A_1R

Because amino acids Pro or Gly are involved in helix macroswitches [48], mutation of these structural residues can result in misfolding and degradation of the receptor. We first assessed the impact of the G279$^{7.44}$S mutation on A_1R expression and plasma membrane targeting. Both A_1R^{wt} and A_1R^{G279S} stably expressed in HEK-293 T cells showed a comparable subcellular distribution (Fig. 1B). Cell-surface A_1R^{wt} and A_1R^{G279S} were isolated after biotinylation and the amount of plasma membrane receptors, as a fraction of the total in the cell lysate, was determined by immunoblotting (Fig. 1 C). The results also showed equivalent cell-surface density for both A_1R^{wt} and A_1R^{G279S} (Fig. 1D).

G279$^{7.44}$ is localized in the middle of TM7 of A_1R, facing the lipid bilayer, thus not forming part of the orthosteric binding site (Fig. 1 A) [49]. However, the G279$^{7.44}$S mutation could induce indirect effects at the binding site. Next, we evaluated whether the mutation affected A_1R ligand binding in living cells. To this end, we implemented a NanoBRET-based approach using the fluorescent A_1R antagonist CA200634 [36] (Fig. 2 A). HEK-293 T cells expressing A_1R^{wt} and A_1R^{G279S} were challenged with increasing concentrations of CA200634, in the presence or absence of the nonlabelled A_1R antagonist DPCPX. A similar binding saturation hyperbola was obtained for both A_1R^{wt} (K_D = 147 ± 72 nM and B_{max} = 56 ± 5%) and A_1R^{G279S} (K_D = 128 ± 50 nM and B_{max} = 57 ± 7%), which was displaced in the presence of a saturating concentration of DPCPX (1 μM) (Fig. 2 B and C). Overall, our results demonstrated that A_1R^{G279S}, when stably expressed in living cells, shows an equivalent subcellular distribution and cell surface density as demonstrated by immunofluorescence, biotinylation (i.e., immunoblotting) and NanoBRET (i.e., B_{max}) experiments. Furthermore, our NanoBRET experiments revealed that the plasma membrane A_1R^{G279S} had the same affinity as the wild-type receptor for the fluorescent ligand CA200634.

3.2. Functional coupling of A_1R^{G279S} to transducer proteins

G279$^{7.44}$ is located near the conserved NP$^{7.50}$xxY motif (Fig. 1 A), which is essential to form the receptor active conformation [50]. Therefore, we assessed whether the G279$^{7.44}$S mutation altered the A_1R functional coupling to transducer proteins. To this end, we evaluated agonist-induced real-time functional coupling of the receptor to G proteins, β-arrestin2 or GRK2 through an engineered A_1R NanoLuc Binary Technology (NanoBiT) assay (Fig. 3 A) [37]. A_1R^{wt}-SmBiT or A_1R^{G279S}-SmBiT were transiently expressed in HEK-293 T cells together with the indicated transducer protein fused to the complementary LgBiT subunit (i.e., $G_{\alpha i}$-LgBiT, $G_{\alpha q}$-LgBiT, $G_{\alpha 12/13}$-LgBiT, $G_{\alpha s}$-LgBiT, β-arrestin2-LgBiT or GRK2-LgBiT). Subsequently, the A_1R agonist-induced increase in coelenterazine-induced NL bioluminescent light was recorded (Fig. 3 A). In fact, when HEK-293 T cells expressing A_1R^{wt}-SmBiT and $G_{\alpha i}$-LgBiT or $G_{\alpha q}$-LgBiT were challenged with the A_1R agonist CPA, a rapid increase in the NL-generated signal was observed, reaching a peak at 10 min with a subsequent decline to basal after 1 h (Fig. 3B, left and right panels, respectively). Cells expressing A_1R^{G279S}-SmBiT and $G_{\alpha i}$-LgBiT or $G_{\alpha q}$-LgBiT showed a very similar real-time G protein functional coupling, as compared with cells expressing A_1R^{wt}-SmBiT and $G_{\alpha i}$-LgBiT or $G_{\alpha q}$-LgBiT (Fig. 3B, left panel and right panel, respectively). No functional coupling was observed between A_1R^{wt} or A_1R^{G279S} and other G protein subunits ($G_{\alpha 12/13}$ and $G_{\alpha s}$), β-arrestin2 or GRK2. (Fig. 3 C). Therefore, A_1R^{wt} and A_1R^{G279S} showed a similar transducer protein coupling profile with selectivity for $G_{\alpha i}$ and $G_{\alpha q}$ proteins and without avidity for $G_{\alpha 12/13}$, $G_{\alpha s}$, β-arrestin2 or GRK2 (Fig. 3 C). Finally, we performed concentration-response experiments to assess whether the G279$^{7.44}$S mutation affected the potency of A_1R agonist-induced coupling to $G_{\alpha i}$ protein. CPA induced a concentration-dependent increase in the functional coupling to $G_{\alpha i}$ both in A_1R^{wt} and A_1R^{G279S} without significant differences in the potencies (A_1R^{wt} pEC_{50} = 7.79 (7.62–7.99, 95% CI); A_1R^{G279S} pEC_{50} = 7.76 (7.49–8.05, 95% CI); n = 4; $F_{(1,46)}$ = 0.065, P = 0.8) (Fig. 4 A). Overall, the G279$^{7.44}$S mutation does not cause any bias in A_1R signalling profile or modifies agonist potency or efficacy.

There is contradictory evidence for the existence of A_1R constitutive activity in native tissues [51], although it can be demonstrated in heterologous expression systems with the use of A_1R inverse agonists, such as DPCPX [54,55]. Therefore, we evaluated whether the G279$^{7.44}$S mutation affects the A_1R constitutive activity in living cells, by

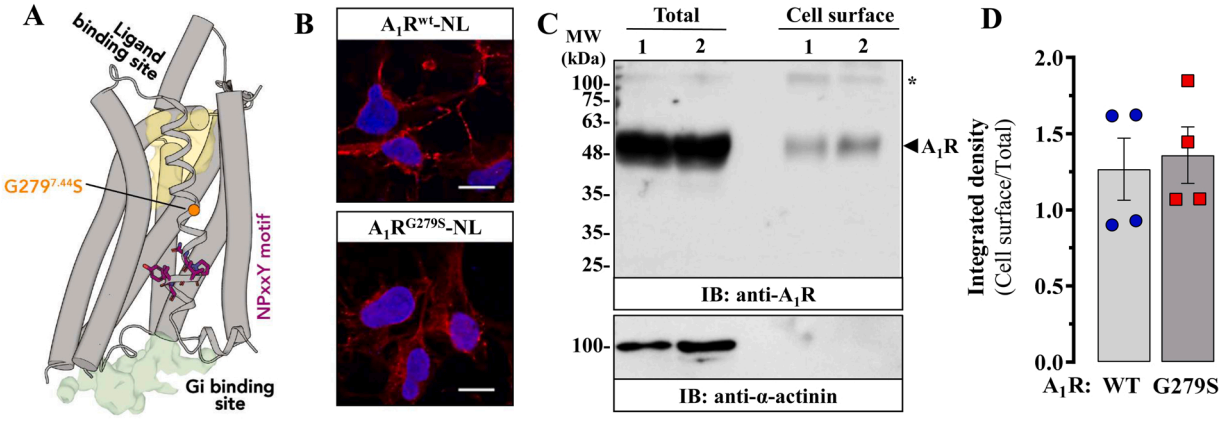

Fig. 1. Expression of A_1R^{wt} and A_1R^{G279S} in HEK-293 T cells. (A) Cryo-EM structure of A_1R (PDB id 6D9H) [66] showing the positions of G279$^{7.44}$ (orange circle) within TM 7, the highly conserved NP$^{7.50}$xxY motif (purple sticks), the adenosine orthosteric binding site (yellow surface), and the Gi binding site (green surface). **(B)** Immunofluorescence detection of A_1R^{wt}-NL and A_1R^{G279S}-NL in stable transfected HEK-293 T cells. Cells stably expressing A_1R^{wt}-NL and A_1R^{G279S}-NL were processed for immunocytofluorescence detection of A_1R (red) using a rabbit anti-A_1R (1 μg/ml) antibody. Nuclei were stained with DAPI (blue) (see Methods). Scale bar: 10 μm. **(C)** Representative immunoblot showing total and cell surface density of A_1R^{wt}-NL (lane 1) and A_1R^{G279S}-NL (lane 2) in stable transfected HEK-293 T cells. Total and cell surface extracts were analysed by SDS-PAGE and immunoblotted using rabbit anti-A_1R (1 μg/ml) antibody (see Methods). The asterisk denotes the possible identification of the A_1R homodimer, as previously described [67]. **(D)** Relative quantification of A_1R^{wt}-NL and A_1R^{G279S}-NL cell surface density. The immunoblot protein bands corresponding to A_1R^{wt}-NL and A_1R^{G279S}-NL were quantified by densitometric scanning; values were normalized to the respective amount of α-actinin in each lane to correct for protein loading in the total extract. Then, the densitometric scanning of cell surface A_1R^{wt}-NL and A_1R^{G279S}-NL was related to the normalized total amount of receptor (Cell surface/Total) and expressed as mean ± SEM of four independent experiments. No significant difference was observed in cell surface expression between A_1R^{wt}-NL and A_1R^{G279S}-NL (p = 0.7516, Student t test).

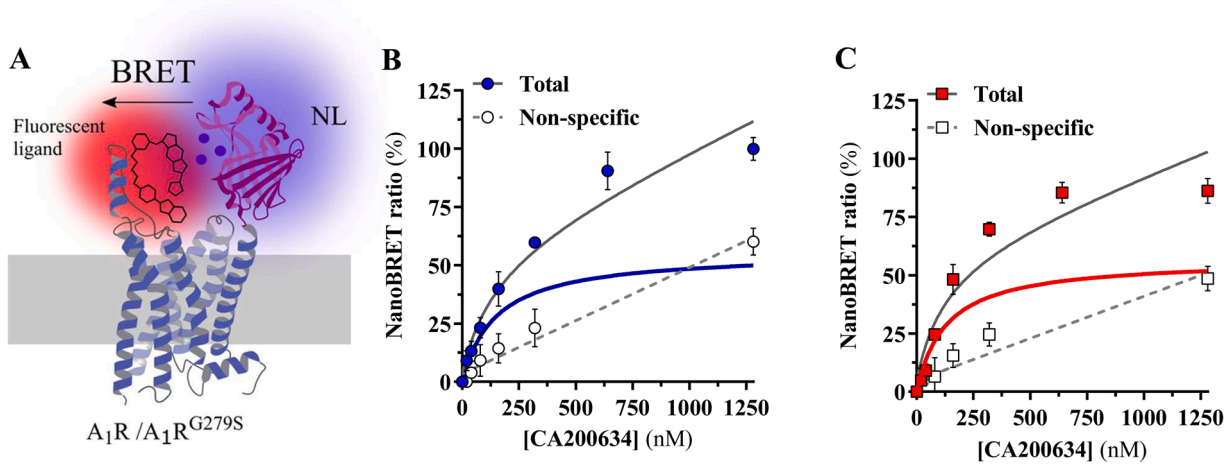

Fig. 2. A_1R cell surface ligand binding determinations. (A) Schematic representation of the NanoBRET assay. Nanoluciferase (NL) fused to the N-terminal domain of A_1R (i.e., A_1R^{wt}-NL and A_1R^{G279S}-NL) acts as a donor in a bioluminescence resonance energy transfer (BRET) process emitting light at 490–10 nm in presence of coelenterazine 400a (blue circles). The fluorescent ligand (i.e., CA200634) acts as acceptor of the BRET process, thus the light excites the BODIPY attached to the ligan, which subsequently emits fluorescence at 650–80 nm. HEK-293 T cells expressing A_1R^{wt}-NL **(B)** and A_1R^{G279S}-NL **(C)** were incubated with increasing concentrations of CA200634 in the absence (Total) or presence (Non-specific) of 1 μM DPCPX and the fluorescent ligand binding was determined by NanoBRET (*see* Materials and Methods). Results are expressed as mean ± SEM of three independent experiments performed in triplicate.

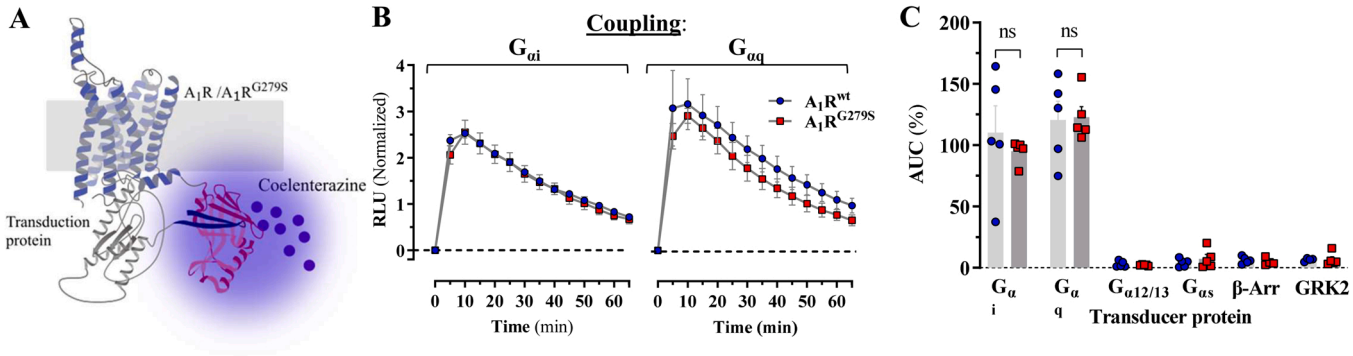

Fig. 3. Agonist-induced receptor/transducer proteins coupling does not differ between A_1R^{wt} and A_1R^{G279S}. (A) Schematic representation of the NanoBiT assay. Nanoluciferase (NL) SmBiT and LgBiT complementary fragments are fused to A_1R^{wt} or $A_1R^{wt/G279S}$ and the different transduction proteins, respectively. As the agonist induce receptor`s coupling to transduction proteins, the NL subunits reconstitute an active NL, which becomes a real-time light reported of receptors' coupling. **(B)** Representative real-time profiles of agonist-induced receptor coupling to $G_{\alpha i}$ and $G_{\alpha q}$. HEK-293 T cells expressing A_1R^{wt}-SmBiT (blue circles) or A_1R^{G279S}-SmBiT (red squares) plus $G_{\alpha i}$-LgBiT (left panel) and $G_{\alpha q}$-LgBiT (right panel) were challenged with CPA (200 nM) and the receptor/G protein coupling was determined by NanoBiT (*see* Materials and Methods). Data show the NL bioluminescent signal after subtracting the vehicle signal and normalizing by basal signal (before CPA addition). Results are expressed as mean ± SD of one representative experiment. **(C)** Quantification of the overall coupling of A_1R^{wt}-SmBiT (blue circles) or A_1R^{G279S}-SmBiT (red squares) to $G_{\alpha i/o}$-LgBiT, $G_{\alpha q}$-LgBiT, $G_{\alpha 12/13}$-LgBiT, $G_{\alpha s}$-LgBiT, β-arrestin2-LgBiT and GRK2-LgBiT as indicated in panel B. Results are shown as percentage of the area under the curve (AUC) extracted from the real-time NanoBiT profiles (shown in panel B).
(a) The A_1R structure (in light blue; adapted from PDB: 5N2S) coupled to the mini-$G_{\alpha o}$ protein (in grey; adapted from [68]) is shown. (b) Also, the structures of the SmBiT and LgBiT are shown in dark blue and purple, respectively (adapted from PDB: 5IBO).

performing concentration-response experiments of inverse agonist-induced uncoupling to $G_{\alpha i}$ protein. DPCPX concentration-dependently reduced the constitutive activity of both A_1R^{wt} and A_1R^{G279S} without significant differences in potency (A_1R^{wt} $pEC_{50} = 7.06$ (6.52–7.63, 95% CI); A_1R^{G279S} $pEC_{50} = 7.08$ (6.63–7.53, 95% CI); $n = 3$; $F_{(1,46)} = 0.006$, $P = 0.94$) (Fig. 4B), indicating that the G279S mutation does not affect the constitutive activity of heterologously expressed A_1R.

3.3. *Molecular dynamics of the G279$^{7.44}$S mutation in A_1R*

The lack of side chain in Gly might facilitate local helix flexibility, changing the collective dynamics of the helix [52]. However, the short side chain of Ser may also induce local structural distortions by forming a hydrogen bond interaction with the carbonyl backbone in the previous turn of the helix in the χ_1 rotameric *gauche-* (*g-*) or *gauche+* (*g+*) states [53,54]. Therefore, we evaluated and compared the flexibility and conformation of TM 7 in A_1R^{wt} and A_1R^{G279S} by molecular dynamic (MD) simulations. We performed independent replicas of unrestrained MD trajectory of A_1R^{wt} (3 ×1 μs) and A_1R^{G279S} with initial *g-* (2 ×1 μs) or *g+* (2 ×1 μs) conformation of S279$^{7.44}$ (see Methods). S279$^{7.44}$ in A_1R^{G279S} can populate both the *g+* and *g-* rotameric states independently of the initial *g-* (58% in *g-*, 42% in *g+*) or *g+* (64% in *g-*, 36% in *g+*) state (Supplementary Fig. S1A). For simplicity, we combined the results of the *g+* and *g-* simulations with a total aggregate sampling of 4 μs for the A_1R^{G279S}. The flexibility of TM helices and loops was characterized by the root-mean-square fluctuation (RMSF). As expected, loops are more flexible than TM helices, but, importantly, average RMSF values and associated B-factor values are similar in the I272$^{7.37}$-I286$^{7.51}$ stretch of amino acids (two helical turns before and after the 279$^{7.44}$ position) in A_1R^{wt} and A_1R^{G279S} (Fig. 5 A). A more detailed analysis of twist angles (see Methods) shows no significant differences (Fig. 5B). These simulations also showed that the position of the extracellular part

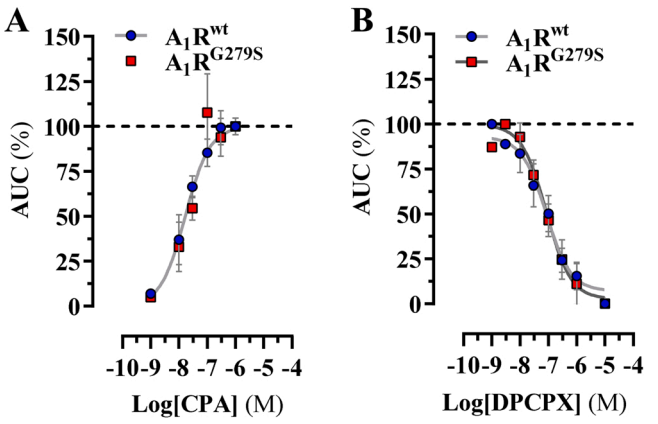

Fig. 4. Ligand-induced concentration-response curves of $A_1R/G_{\alpha i}$ protein coupling. HEK-293 T cells expressing A_1R^{wt}-SmBiT (blue circles) or A_1R^{G279S}-SmBiT (red squares) plus $G_{\alpha i}$-LgBiT were challenged with increasing concentrations of CPA (**A**) or DPCPX (**B**) and the receptor/$G_{\alpha i}$ protein coupling was determined by NanoBiT (*see* Materials and Methods). Results are shown as percentage of the area under the curve (AUC) for each CPA and DPCPX concentration induced real-time NanoBiT profile (*see* Fig. 3B) and expressed as mean ± SEM of four and three independent experiments each performed in triplicate, respectively.

of TM 7, which could influence ligand binding, is not altered in A_1R^{G279S} relative to A_1R^{wt} (Supplementary Fig. S1D), in line with no changes in experimental binding affinities (Fig. 2B-2 C). The active conformation of A_1R for G protein binding requires an intracellular outward movement of TM 6 and an opening of the last turn of TM 7 [50]. Thus, we also calculated the position of the cytoplasmic ends of TMs 6 and 7 in the simulations. Consistent with no changes in the constitutive activity of A_1R (Fig. 4) or the coupling to transducer proteins (Figs. 3 and 4), these intracellular parts of TMs 6 and 7 are not altered in A_1R^{G279S} relative to A_1R^{wt} (Supplementary Figs. S1C-S1E).

The only observed change between A_1R^{wt} and A_1R^{G279S} is at the top of TM 6 (Fig. 5 C and Supplementary Fig. S1B). Surprisingly, the $G279^{7.44}S$ mutation in the middle of TM 7 triggers an inward movement of the extracellular part of TM 6. This indirect mechanism occurs via $S246^{6.47}$. Class A G protein-coupled receptors (GPCRs) contain the highly conserved $CWxP^{6.50}$ motif, while A_1R replaces Cys by Ser to form the $SWxP^{6.50}$ motif (Fig. 5D). The $S246^{6.47}T$ mutation has been associated with invasive breast carcinoma [55]. During computer simulations, the side chain of $S246^{6.47}$ forms a water-mediated hydrogen bond with the side chain of $S279^{7.44}$ in A_1R^{G279S} that does not occur with $G279^{7.44}$ in A_1R^{wt} (Fig. 5E). GPCRs contain internal water molecules that play both a structural and functional role [56–58]. Importantly, a highly conserved water molecule energetically stabilizes the strong $Pro^{6.50}$-kink distortion in TM 6 of class A GPCRs by forming hydrogen bonds with the carbonyl backbone at position 6.47 and the N-H amide backbone at position 6.51 (Fig. 5E). The presence of unusual polar side chains in this environment, $S246^{6.47}$ of the receptor specific $SWxP^{6.50}$ motif of A_1R and $S279^{7.44}$ of A_1R^{G279S}, allows an additional discrete water molecule to interact with these singular $S246^{6.47}$ and $S279^{7.44}$ side chains (24% of the simulation time). As a result, average RMSF values and associated B-factor values are similar (Fig. 5 A) in the $I239^{6.40}$-$L253^{6.54}$ stretch of amino acids (two helical turns before and after $S246^{6.47}$) in A_1R^{wt} and A_1R^{G279S} but, importantly, the pattern of twist angles in this stretch of amino acids increases to values closer to an ideal α-helix (3.6 residues per turn, twist = 100°) in A_1R^{G279S}. Thus, the Pro-induced, water-mediated, bend of TM 6 decreases in A_1R^{G279S} relative to A_1R^{wt}, triggering the inward movement of the extracellular part of TM 6. However, although TM 6, and specially $N254^{6.55}$, forms part of the orthosteric binding site (Fig. 1 A), the ligand binding affinity was not altered in A_1R^{G279S} relative to A_1R^{wt}. We hypothesized that incorporation of this modest conformational change in the middle of TM 6 ($SWxP^{6.50}$) results in a significant displacement of only the residues located at the end of the helix (Fig. 5 C), near the extracellular part, while the magnitude of this displacement at the orthosteric binding site is smaller, due to the proximity to $S246^{6.47}$.

3.4. Impact of the $G279^{7.44}S$ mutation in the formation and function of A_1R-$A_{2A}R$ heteromer

A_1R heteromerizes with $A_{2A}R$ in heterologous expression systems and in the brain, at the striatal glutamatergic terminals [20], producing an adenosine concentration sensor that regulates glutamate neurotransmission [25,59]. Therefore, we evaluated the impact of the $G279^{7.44}S$ mutation on A_1R-$A_{2A}R$ heteromerization and function in living cells. First, A_1R-$A_{2A}R$ heteromer formation was determined using the NanoBiT assay in HEK-293 T cells transiently transfected with $A_{2A}R$-LgBiT plus A_1R^{wt}-SmBiT or A_1R^{G279S}-SmBiT. As expected, when $A_{2A}R$-LgBiT and A_1R^{wt}-SmBiT were co-expressed in HEK-293 T cells a significant heteromerization was observed (Fig. 6 A). Interestingly, the A_1R-$A_{2A}R$ heteromer formation was significantly reduced when $A_{2A}R$-LgBiT was expressed with A_1R^{G279S}-SmBiT (Fig. 6 A), indicating that the A_1R mutation may affect the A_1R-$A_{2A}R$ intermolecular interactions.

Next, we assessed the impact of $G279^{7.44}S$ A_1R mutation on A_1R-$A_{2A}R$ heteromer function. Different allosteric interactions have been described in the A_1R-$A_{2A}R$ heteromer [24,59], including a ligand-independent type II allosteric interaction [13], by which A_1R heteromerization reduces $A_{2A}R$ constitutive activity [24]. Therefore, we expect these interactions to be reduced with A_1R^{G279S} because of its reduced heteromerization with $A_{2A}R$. As previously described [24], the expression of $A_{2A}R$ in HEK-293 T cells significantly increased basal cAMP levels (11.8 ± 2.6% over mock transfected cells) (Fig. 6B), thus indicating the existence of an agonist-independent (i.e., constitutive) activation of adenylyl cyclase. As expected, co-transfection with A_1R^{wt} precluded $A_{2A}R$ constitutive activity, while A_1R^{G279S} co-expression was unable to block $A_{2A}R$ agonist-independent activity (Fig. 6B). We also analysed the previously unexplored possibility that a type II allosteric modulation in the A_1R-$A_{2A}R$ heteromer would also apply to agonist-induced $A_{2A}R$ activation, and we performed concentration-response curves of cAMP accumulation induced by the selective $A_{2A}R$ agonist CGS21680 in the absence and presence of A_1Rs. CGS21680 induced a concentration-dependent increase in cAMP accumulation (pEC_{50} = 8.3 (7.8–8.7, 95% CI); E_{max} = 80.9% (68.3–96.8, 95% CI) (Fig. 6 C) and, when A_1R^{wt} was cotransfected, a significant reduction was obeserved in the efficacy of the $A_{2A}R$ agonist (E_{max} = 60.4% (49.6–76.2, 95% CI); n = 4; $F_{(1,19)} = 6.3$, $P = 0.02$) and potency (pEC_{50} = 7.9 (7.5–8.3, 95% CI); n = 4; $F_{(1,19)} = 4.8$, $P = 0.04$) compared with cells transfected only with $A_{2A}R$ (Fig. 7 C). On the other hand, no significant differences in efficacy (E_{max} = 83.2% (69.1–102.5, 95% CI); n = 4; $F_{(1,18)} = 0.2$, $P = 0.7$) or potency (pEC_{50} = 8.2 (7.7–8.6, 95% CI); n = 4; $F_{(1,18)} = 0.2$, $P = 0.6$) were found in cells cotransfected with A_1R^{G279S}, compared to cells only expressing $A_{2A}R$ (Fig. 6 C). In summary, and as expected from the reduced ability of A_1R^{G279S} to heteromerize with $A_{2A}R$, the heteromerization-dependent ability of A_1R to allosterically decrease in a ligand-independent manner (type II allosterism) both the constitutive and an agonist-induced activation of $A_{2A}R$ disappear with A_1R^{G279S}, with its specific inability to heteromerize with $A_{2A}R$.

3.5. Molecular dynamic simulations of the $G279^{7.44}S$ mutation and A_1R-$A_{2A}R$ heteromerization

Previously reported bimolecular fluorescence complementation (BiFC) experiments, in the presence of synthetic peptides corresponding to different TM domains of A_1R and $A_{2A}R$, revealed that the A_1R-$A_{2A}R$ heteromer interface is formed by TMs 5 and 6 (TM 5/6 interface) [59,

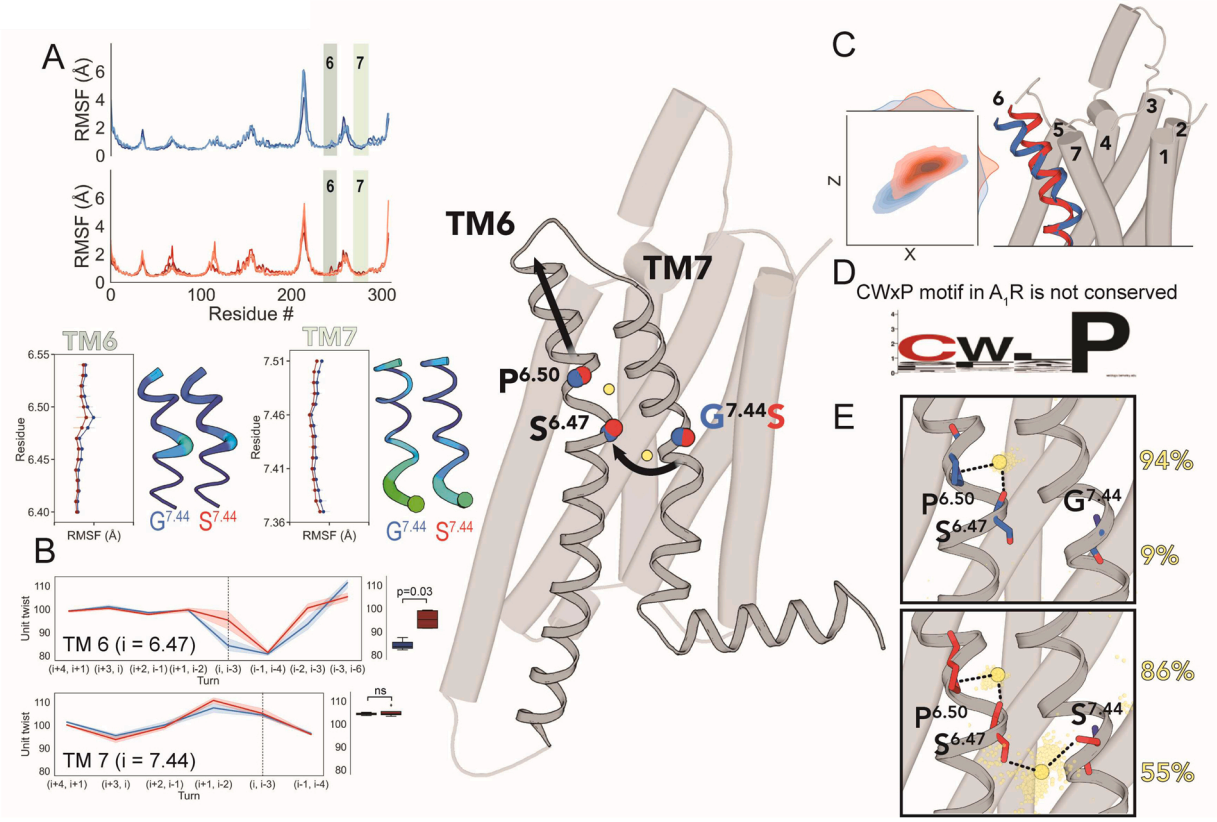

Fig. 5. Computational simulations of A_1R^{wt} and A_1R^{G279S}. (**A**) Average root-mean-square fluctuation (RMSF) during 1 μ s unrestrained MD simulations of A_1R^{wt} (3 replicas in blue) and A_1R^{G279S} (4 replicas in red). Detailed view of average RMSF and associated B-factor values in the $I239^{6.40}$-$L253^{6.54}$ (left) and $I272^{7.37}$-$I286^{7.51}$ (right) stretch of amino acids (two helical turns before and after $S246^{6.47}$ or $G/S279^{7.44}$, respectively). (**B**) Average unit twist angles (see Methods) along these stretches of amino acids in which position i was assigned to either $S246^{6.47}$ (left) of $G/S279^{7.44}$ (right) in A_1R^{wt} and A_1R^{G279S}. Boxplots of unit twist angles at the (i, i-3) turn of TMs 6 and 7 (broken line). Statistical significance was calculated by non-parametric Mann−Whitney test. (**C**) Contour plots of the evolution of the center of mass of amino acids $T257^{6.58}$-$C260^{6.61}$ in TM 6 during the MD simulations of A_1R^{wt} and A_1R^{G279S}. The xy plane is as defined by the Orientations of Proteins in Membranes (OPM) [69]. Distributions of the x and y values are shown on the right x-axis and top y-axis, respectively. The inward movement of the top of TM 6 is illustrated in the right panel. (**D**) Sequence logo of class A GPCRs showing the highly conserved $CWxP^{6.50}$ motif. A_1R replaces Cys by Ser to form the receptor specific $SWxP^{6.50}$ motif. (**E**) Detailed views of a water-mediated hydrogen bond between $S246^{6.47}$ and $S279^{7.44}$ in A_1R^{G279S} (bottom panel) and a highly conserved water molecule that energetically stabilizes the strong $Pro^{6.50}$-kink distortion in TM 6 of class A GPCRs by forming hydrogen bonds with the backbone carbonyl at position 6.47 and the backbone N-H amide at position 6.51 present in both A_1R^{wt} (top) and A_1R^{G279S} (bottom). The percentage of presence of these water molecules are shown.

60]. MD simulations of the A_1R^{wt}-$A_{2A}R$ heteromer (3 ×1 μs) and the putative A_1R^{G279S}-$A_{2A}R$ (3 ×1 μs) heteromer confirmed that the $G279^{7.44}S$ mutation in A_1R^{G279S} triggers an inward movement of the extracellular part of TM 6 relative to A_1R^{wt}, while TM 5 remains unchanged (Fig. 8 A). This change in TM 6 of A_1R^{G279S} modifies the position of the partner TM 5 of $A_{2A}R$, relative to A_1R^{wt} (Fig. 7 A). Two different positions of TM 5 of $A_{2A}R$ are observed in the set of structures collected during the MD simulations, but in both minima a counterclockwise rotation from the extracellular view is observed. Consequently, a concerted movement of TM 6 of $A_{2A}R$ to two minima analogue to those of TM 5 $A_{2A}R$ are also observed (Fig. 7 A). In general, the entire $A_{2A}R$ protomer rotates in a counterclockwise direction, as can be seen from the movement of its mass center (Fig. 7B). This moves away TM 6 of $A_{2A}R$ from TM 5 of A_1R^{G279S}, weakening the TM 5–6 interface and, therefore, providing a molecular explanation for a hindrance of heteromerization.

4. Discussion

An *ADORA1* autosomal-recessive mutation in two Iranian siblings (30 and 34 years old) with consanguine parents has been associated to EOPD [26]. In the present study, we report that while the corresponding $G279^{7.44}S$ mutation does not affect A_1R expression and signalling, it reduces the ability of the receptor to heteromerize with $A_{2A}R$ and, therefore, the ability of A_1R to exert a negative allosteric modulation of $A_{2A}R$. Results from computational simulations provided compelling evidence supporting that $G279^{7.44}S$ triggers structural changes in the TM 5/6 interface of the A_1R-$A_{2A}R$ heteromer that determine a hindrance of heteromerization. Therefore, it is shown that a PD linked *ADORA1* mutation is associated with dysfunction of adenosine receptor heteromerization.

The description of inherited monogenic diseases and subphenotypes associated with GPCR mutations increased significantly in the past decade [61]. Mostly, these mutations trigger a GPCR gain- or loss-of-function, but also other receptor dysfunctions such us biased signalling, ectopic expression, pseudogenization and/or trans-signalling have been reported [61]. In the case of the *ADORA1* mutation both subjects present a homozygous missense mutation (c 0.835 G>A), yet alterations in main PD-related genes (i.e., *PRKN*, *PINK1* and *DJ-1*) were not observed [26]. The pathogenic effect of this *ADORA1* mutation on PD and its implications for EOPD are a matter of debate [28]. For example, it has been postulated that it is related to changes in the functional interactions of A_1R with the dopamine D_1 receptor (D_1R) [26, 27]. It has also been suggested that the interaction of two or more genetic loci, which can significantly alter disease severity ("genetic modifiers"), or result in completely new phenotypes, could be behind the

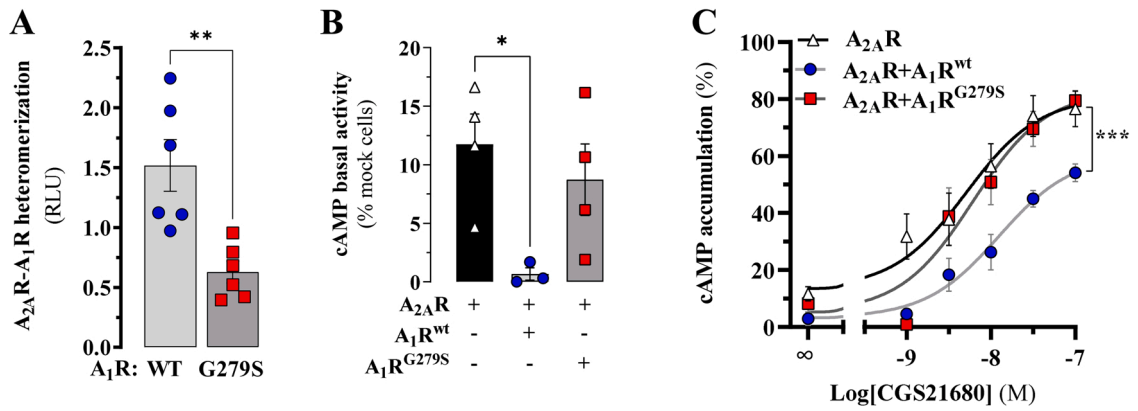

Fig. 6. Impact of G279$^{7.44}$S mutation on $A_1R/A_{2A}R$ heteromerization. (A) A_1R-$A_{2A}R$ heteromer formation in living cells. HEK-293 T cells transiently transfected with $A_{2A}R$-LgBiT and A_1R^{wt}-SmBiT or A_1R^{G279S}-SmBiT were processed for NanoBiT assay. The NanoBiT signal (RLU) was normalized by co-transfected CFP (fluorescence). Results are expressed as mean ± SEM of six independent experiments performed in quadruplicates. * * $P < 0.01$ Student *t*-test. **(B)** Constitutive activation of adenylyl cyclase by $A_{2A}R$. HEK-293 T cells permanently expressing $A_{2A}R$-NL were transiently transfected with $A1R^{wt}$, $A1R^{G279S}$ or empty vector (mock) and the basal cAMP accumulation determined as described in Materials and Methods. Results were normalized by the basal cAMP accumulation in mock transfected cells and expressed as means ± SEM of the of four independent experiments each performed in triplicate. * $P < 0.05$, one-way ANOVA with Tukey's *post-hoc* test. **(C)** $A_{2A}R$ agonist-induced concentration-response curves of cAMP accumulation. HEK-293 T cells transfected as descried in panel B were challenged with increasing concentrations of CGS21680 and the cAMP accumulation determined as described in Materials and Methods. Results were normalized by the basal cAMP accumulation in mock transfected cells and expressed as means ± SEM of the of four independent experiments each performed in triplicate. $^{\#}(F_{(6,56)} = 8.368)$ $P < 0.0001$, extra sum-of-squares F test.

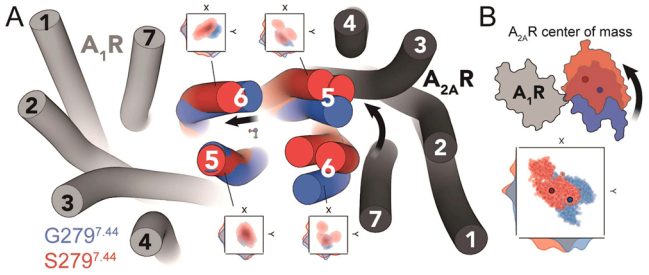

Fig. 7. Representative structures obtained in MD simulations of the A_1R^{wt}-$A_{2A}R$ and A_1R^{G279S}-$A_{2A}R$ heteromers. (A) The movement of TMs 5 & 6 forming the TM 5/6 interface (blue for $A_1R^{wt}/A_{2A}R$ and red for $A_1R^{G279S}/A_{2A}R$) is shown, whereas the other TM helices correspond to the initial model (in gray). Evolution of the center of mass of amino acids M177$^{5.35}$-Y182$^{5.40}$ in TM 5 and T257$^{6.58}$-C260$^{6.61}$ in TM 6 of either A_1R^{wt} or A_1R^{G279S} and P173$^{5.34}$-F180$^{5.41}$ in TM 5 and N253$^{6.55}$-F258$^{6.60}$ in TM 6 of $A_{2A}R$ during three replicas of unbiased 1 μs MD simulations (100 structures collected every 10 ns in each replica) and their distributions. The xy plane is defined as in Fig. 6. **(B)** The movement of $A_{2A}R$ relative to A_1R^{wt} or A_1R^{G279S} within the heteromer was monitored by the center of mass of $A_{2A}R$ in the MD simulations of the $A_1R^{wt}/A_{2A}R$ and $A_1R^{G279S}/A_{2A}R$ heteromers. Black arrows represent the movement of TM helices in the presence of the single point G279$^{7.44}$S mutation (A_1R^{G279S}, in red) relative to wild type sequence (A_1R^{wt}, in blue).

pathological association of the *ADORA1* mutation with PD. It is noteworthy that there are many reports that GPCR mutations are genetic modifiers of human diseases [61]. In such a case, although the GPRC variant does not cause the disease, it represents a risk factor and a modifier of the disease, thus eventually responding to environmental factors, stress, and drugs [61].

Gly at position 7.44 is not conserved among all class A GPCRs. It is present in the A_1R, but not in the $A_{2A}R$ or $A_{2B}R$. It is also present in the neuromedin-B receptor, the neuropeptide FF receptor 2, the urotensin-2 receptor, the glucose-dependent insulinotropic receptor GP119, and the orphan receptor GPR22 [62]. Because Gly residues are involved in macroswitches [48], Gly$^{7.44}$ could be a unique structural and functional signature for these receptors. However, mutating this Gly residue did not have any consequence on the function of A_1R in terms of total and plasma membrane expression (Fig. 1), ligand binding (Fig. 2), coupling to transducer proteins (Figs. 3–4) or intrinsic constitutive activity (Fig. 4B).

Since A_1R forms functionally and pharmacologically significant heteromers with $A_{2A}R$ [20,59] we questioned whether the G279$^{7.44}$S mutation could have an impact on A_1R-$A_{2A}R$ heteromerization. In fact, using a NanoBiT assay in transfected HEK-293 T cells, it could be shown that A_1R^{G279S} loses its ability to heteromerize with $A_{2A}R$, leading to the disappearance of the heteromerization-dependent negative allosteric modulation that A_1R imposes on the constitutive activity and agonist-induced activation of the $A_{2A}R$.

One main localization of A_1R-$A_{2A}R$ heteromers is in the terminals of corticostriatal neurons [20]. Recent studies suggest that changes in the stoichiometry of A_1Rs and $A_{2A}R$s in favor of $A_{2A}R$s secondary to brain iron deficiency are associated with an increase in the sensitivity of these terminals to release glutamate [63]. It was hypothesized that this would depend on an unleashed constitutive activity of $A_{2A}R$s not forming heteromers with A_1Rs. We have suggested that this may be a pathogenetic mechanism secondary to the brain iron deficiency associated with restless legs syndrome, where the $A_1R/A_{2A}R$ stoichiometric change is due to downregulation of A_1Rs and possible upregulation of $A_{2A}R$ [63,64]. Therefore, a greater increase in the sensitivity of the striatal glutamatergic terminals should then be expected in subjects with the G279$^{7.44}$S *ADORA1* mutation, where a higher proportion of $A_{2A}R$s would not form heteromers with A_1R. The consequent hyperglutamatergic state could then play an important favoring pathogenetic mechanism in the development of EOPD. It is important to realize that $A_{2A}R$ free from A_1R should also be able to modify its other potential interactions with other proteins present in the striatal glutamatergic terminal, which includes other GPCRs, such as the CB_1R [24], and other adenosine receptor interacting proteins (ARIPs), including cytoskeleton-related proteins, such as α-actinin (reviewed in [65]). Modifications on those interactions could also play a significant additional role in the functional differences between $A_{2A}R$ forming and not forming heteromers with A_1R. However, when heteromers are formed with CB_1R, nevertheless, the $A_{2A}R$ shows significant constitutive activity [24].

An additional finding of the present study was the demonstration of a type II allosteric mechanism [13] by which A_1R-$A_{2A}R$ heteromerization leads to a significant decrease in the efficacy and potency of an $A_{2A}R$ agonist (CGS21680). If the same mechanism would apply to the

endogenous neurotransmitter, this would imply a further separation of the already lower affinity of adenosine for $A_{2A}R$ compared to A_1R in the corticostriatal terminal. In fact, in a recent study using an in vivo optogenetic-microdialysis technique in rats, increasing the extracellular concentration of adenosine with the local application of dipyridamole, an inhibitor of equilibrative nucleoside transporters, led only to the activation of A_1Rs, with a significant decrease in basal and optogenetic-induced corticostriatal glutamate release [64]. An increased sensitivity to adenosine of $A_{2A}R$ not forming heteromers with A_1R could then also contribute to our previously postulated hyperglutamatergic state of the EOPD associated with the $G279^{7.44}S$ *ADORA1* mutation [69]. Therefore, the administration of $A_{2A}R$ inverse agonists, which would block both the effect of endogenous adenosine and the $A_{2A}R$ constitutive activity, could provide a protective effect in the development of the disease.

Funding

Supported by projects PID2019–109240RB-I00 and PID2020–118511RB-I00 founded by MCIN/AEI/ 10.13039/ 501100011033, "ERDF A way of making Europe", The Michael J. Fox Foundation (MJFF-001051) and Generalitat de Catalunya (2017SGR1604) to FC. Also supported by "Acció instrumental de formació de científics i tecnòlegs" (SLT017/20/000114) of the Departament de Salut de la Generalitat de Catalunya. Grant PRE2018–084480 founded by MCIN/AEI /10.13039/501100011033 "ESF Investing in your future" to JA. CLT is recipient of a FPI fellowship (BES-2017–081872). SF is supported by the intramural funds of the National Institute on Drug Abuse (grant ZIA DA000493). The study was also supported by the Luxembourg Institute of Health (LIH), Luxembourg National Research Fund (INTER/FNRS grants 20/15084569) and F.R.S.-FNRS-T é lévie (grants 7.4593.19, 7.4529.19 and 7.8504.20).

CRediT authorship contribution statement

Laura I. Sarasola: Data curation, Methodology. **Claudia Llinas del Torrent:** Data curation, Methodology. **Andrea P é rez-Arévalo:** Methodology. **Josep Argerich:** Methodology **Nil Casajuana-Martín:** Methodology. **Andy Chevigné:** Investigation. **Víctor Fernández-Dueñas:** Supervision, Editing. **Sergi Ferré:** Writing – reviewing and editing. **Leonardo Pardo:** Writing – reviewing and editing. **Francisco Ciruela:** Conceptualization, Writing – reviewing and editing.

Conflict of interest statement

The authors declare that they have no known competing financial interests or personal relationships that could have appeared to influence the work reported in this paper.

Data availability

Data will be made available on request.

Acknowledgements

We thank Esther Castaño and Benjamín Torrejón from the CCiT-Bellvitge Campus of the University of Barcelona. The authors thank the Centres de Recerca de Catalunya (CERCA) Programme/Generalitat de Catalunya for IDIBELL institutional support and Maria de Maeztu MDM-2017–0729 to Institut de Neurociencies, Universitat de Barcelona.

Authors' contributions

LS, performed biochemical, immunostaining and NanoBiT experiments; AP-A, performed NanoBRET experiments; JA made plasmid constructs and NanoBiT experiments; CLT and NC-M, performed computational studies; AC, made plasmid constructs and revised the manuscript; VF-D, performed NanoBRET experiments and revised the manuscript; SF, conceive the experiments and revised the manuscript; LP, SF, conceive structural experiments and revised the manuscript; FC, conceive the experiments, analyse results and wrote the manuscript.

Appendix A. Supporting information

Supplementary data associated with this article can be found in the online version at doi:10.1016/j.biopha.2022.113896.

References

[1] L.V. Kalia, A.E. Lang, Parkinson's disease, Lancet 386 (2015) 896–912, https://doi.org/10.1016/S0140-6736(14)61393-3.
[2] W. Poewe, K. Seppi, C.M. Tanner, G.M. Halliday, P. Brundin, J. Volkmann, A.-E. Schrag, A.E. Lang, Parkinson disease, Nat. Rev. Dis. Prim. 3 (2017) 17013, https://doi.org/10.1038/nrdp.2017.13.
[3] O.B. Tysnes, A. Storstein, Epidemiology of Parkinson's disease, J. Neural Transm. 124 (2017) 901–905, https://doi.org/10.1007/s00702-017-1686-y.
[4] L.M. de Lau, M.M. Breteler, Epidemiology of Parkinson's disease, Lancet Neurol. 5 (2006) 525–535, https://doi.org/10.1016/S1474-4422(06)70471-9.
[5] A. Schrag, J.M. Schott, Epidemiological, clinical, and genetic characteristics of early-onset parkinsonism, Lancet Neurol. 5 (2006) 355–363, https://doi.org/10.1016/S1474-4422(06)70411-2.
[6] M.J. Barrett, N.E. Hac, G. Yan, M.B. Harrison, G.F. Wooten, Relationship of age of onset and family history in Parkinson disease, Mov. Disord. 30 (2015) 733–735, https://doi.org/10.1002/MDS.26166.
[7] L.W. Ferguson, A.H. Rajput, A. Rajput, Early-onset vs. Late-onset Parkinson's disease: A Clinical-pathological Study, Can. J. Neurol. Sci. 43 (2015) 113–119, https://doi.org/10.1017/cjn.2015.244.
[8] W. Poewe, Treatments for Parkinson disease–past achievements and current clinical needs, Neurology 72 (2009) S65–S73, https://doi.org/10.1212/WNL.0b013e31819908ce.
[9] J.G. Nutt, N.I. Bohnen, Non-dopaminergic therapies, J. Park. Dis. 8 (2018) S73–S78, https://doi.org/10.3233/JPD-181472.
[10] A. Vallano, V. Fernández-Dueñas, C. Pedrós, J.M. Arnau, F. Ciruela, An update on adenosine A2A receptors as drug target in Parkinson's Disease, CNS Neurol. Disord. Drug Targets 10 (2011).
[11] J.F. Chen, R.A. Cunha, The belated US FDA approval of the adenosine A 2A receptor antagonist istradefylline for treatment of Parkinson's disease, Purinergic Signal 16 (2020) 167–174, https://doi.org/10.1007/S11302-020-09694-2.
[12] S. Ferré, J. Bonaventura, W. Zhu, C. Hatcher-Solis, J. Taura, C. Quiroz, N.-S. Cai, E. Moreno, V. Casadó-Anguera, A. v Kravitz, K.R. Thompson, D.G. Tomasi, G. Navarro, A. Cordomí, L. Pardo, C. Lluís, C.W. Dessauer, N.D. Volkow, V. Casadó, F. Ciruela, D.E. Logothetis, D. Zwilling, Essential Control of the Function of the Striatopallidal Neuron by Pre-coupled Complexes of Adenosine A2A-Dopamine D2 Receptor Heterotetramers and Adenylyl Cyclase, in: Front Pharmacol, 9, 2018, p. 243, https://doi.org/10.3389/fphar.2018.00243.
[13] S. Ferré, F. Ciruela, C.W. Dessauer, J. González-Maeso, T.E. Hébert, R. Jockers, D. E. Logothetis, L. Pardo, G protein-coupled receptor-effector macromolecular membrane assemblies (GEMMAs, Pharm. Ther. 231 (2022), 107977, https://doi.org/10.1016/J.PHARMTHERA.2021.107977.
[14] A.M. Sebastião, J.A. Ribeiro, Adenosine receptors and the central nervous system, Handb. Exp. Pharm. (2009) 471–534, https://doi.org/10.1007/978-3-540-89615-9_16.
[15] S. Ferré, W.T. O'Connor, P. Svenningsson, L. Bjorklund, J. Lindberg, B. Tinner, I. Stromberg, M. Goldstein, S.O. Ogren, U. Ungerstedt, B.B. Fredholm, K. Fuxe, Dopamine D1 receptor-mediated facilitation of GABAergic neurotransmission in the rat strioentopenduncular pathway and its modulation by adenosine A1 receptor-mediated mechanisms, Eur. J. Neurosci. 8 (1996) 1545–1553.
[16] J. Borycz, M.F. Pereira, A. Melani, R.J. Rodrigues, A. Kőfalvi, L. Panlilio, F. Pedata, S.R. Goldberg, R.A. Cunha, S. Ferré, Differential glutamate-dependent and glutamate-independent adenosine A1 receptor-mediated modulation of dopamine release in different striatal compartments, J. Neurochem 101 (2007) 355–363, https://doi.org/10.1111/J.1471-4159.2006.04386.X.
[17] A.M. Sebastiao, J.A. Ribeiro, Fine-tuning neuromodulation by adenosine, Trends Pharm. Sci. 21 (2000) 341–346.
[18] C.V. Gomes, M.P. Kaster, A.R. Tomé, P.M. Agostinho, R.A. Cunha, Adenosine receptors and brain diseases: neuroprotection and neurodegeneration, Biochim Biophys. Acta 2011 (1808) 1380–1399, https://doi.org/10.1016/j.bbamem.2010.12.001.
[19] B.B. Fredholm, J.F. Chen, R.A. Cunha, P. Svenningsson, J.M. Vaugeois, Adenosine and brain function, Int Rev. Neurobiol. 63 (2005) 191–270, https://doi.org/10.1016/S0074-7742(05)63007-3.
[20] F. Ciruela, V. Casado, R.J. Rodrigues, R. Lujan, J. Burgueno, M. Canals, J. Borycz, N. Rebola, S.R. Goldberg, J. Mallol, A. Cortes, E.I. Canela, J.F. Lopez-Gimenez, G. Milligan, C. Lluis, R.A. Cunha, S. Ferre, R. Franco, Presynaptic control of striatal glutamatergic neurotransmission by adenosine A1-A2A receptor heteromers, J. Neurosci. 26 (2006) 2080–2087, https://doi.org/10.1523/JNEUROSCI.3574-05.2006.

[21] S.G. Ferreira, F.Q. Gonçalves, J.M. Marques, Â.R. Tomé, R.J. Rodrigues, I. Nunes-Correia, C. Ledent, T. Harkany, L. Venance, R.A. Cunha, A. Köfalvi, Presynaptic adenosine A 2A receptors dampen cannabinoid CB 1 receptor-mediated inhibition of corticostriatal glutamatergic transmission, Br. J. Pharm. 172 (2015) 1074–1086, https://doi.org/10.1111/bph.12970.
[22] J. Bonaventura, C. Quiroz, N.-S. Cai, M. Rubinstein, G. Tanda, S. Ferré, Key role of the dopamine D4 receptor in the modulation of corticostriatal glutamatergic neurotransmission, Sci. Adv. 3 (2017), e1601631, https://doi.org/10.1126/sciadv.1601631.
[23] G. Yepes, X. Guitart, W. Rea, A.H. Newman, R.P. Allen, C.J. Earley, C. Quiroz, S. Ferré, Targeting hypersensitive corticostriatal terminals in restless legs syndrome, Ann. Neurol. 82 (2017) 951–960, https://doi.org/10.1002/ANA.25104.
[24] A. Köfalvi, E. Moreno, A. Cordomí, N.S. Cai, V. Fernández-Dueñas, S.G. Ferreira, R. Guixà-González, M. Sánchez-Soto, H. Yano, V. Casadó-Anguera, R.A. Cunha, A. M. Sebastião, F. Ciruela, L. Pardo, V. Casadó, S. Ferré, Control of glutamate release by complexes of adenosine and cannabinoid receptors, BMC Biol. 18 (2020), https://doi.org/10.1186/s12915-020-0739-0.
[25] F. Ciruela, S. Ferre, V. Casado, A. Cortes, R.A. Cunha, C. Lluis, R. Franco, Heterodimeric adenosine receptors: a device to regulate neurotransmitter release, Cell. Mol. Life Sci. 63 (2006) 2427–2431, https://doi.org/10.1007/s00018-006-6216-2.
[26] E. Jaberi, M. Rohani, G.A. Shahidi, S. Nafissi, E. Arefian, M. Soleimani, A. Moghadam, M.K. Arzenani, F. Keramatian, B. Klotzle, J.B. Fan, C. Turk, F. Steemers, E. Elahi, Mutation in ADORA1 identified as likely cause of early-onset parkinsonism and cognitive dysfunction, Mov. Disord. 31 (2016) 1004–1011, https://doi.org/10.1002/mds.26627.
[27] S. Nasrollahi-Shirazi, D. Szöllösi, Q. Yang, E. Muratspahic, A. El-kasaby, S. Sucic, T. Stockner, C. Nanoff, M. Freissmuth, Functional impact of the G279S substitution in the adenosine A 1-receptor (A 1 R-G279S 7.44), a mutation associated with parkinson's disease, MOLPHARM-AR-2020-000003, Mol. Pharm. 98 (2020), https://doi.org/10.1124/MOLPHARM.120.000003.
[28] C. Blauwendraat, M.A. Nalls, M. Federoff, O. Pletnikova, J. Ding, C. Letson, J. T. Geiger, J.R. Gibbs, D.G. Hernandez, J.C. Troncoso, J. Simón-Sánchez, S. W. Scholz, International Parkinson's Disease Genomics Consortium, ADORA1 mutations are not a common cause of Parkinson's disease and dementia with Lewy bodies, Mov. Disord. 32 (2017) 298–299, https://doi.org/10.1002/mds.26886.
[29] E. Elahi, PTRHD1 and possibly ADORA1 mutations contribute to Parkinsonism with intellectual disability, Mov. Disord. 33 (2018) 174, https://doi.org/10.1002/MDS.27126.
[30] B. Carpenter, R. Nehmé, T. Warne, A.G.W. Leslie, C.G. Tate, Structure of the adenosine A(2A) receptor bound to an engineered G protein, Nature 536 (2016) 104–107, https://doi.org/10.1038/NATURE18966.
[31] Q. Wan, N. Okashah, A. Inoue, R. Nehme, B. Carpenter, C.G. Tate, N.A. Lambert, Mini G protein probes for active G protein-coupled receptors (GPCRs) in live cells, J. Biol. Chem. 293 (2018) 7466–7473, https://doi.org/10.1074/JBC.RA118.001975.
[32] M. Meyrath, C.B. Palmer, N. Reynders, A. Vanderplasschen, M. Ollert, M. Bouvier, M. Szpakowska, A. Chevigné, Proadrenomedullin N-Terminal 20 Peptides (PAMPs) Are Agonists of the Chemokine Scavenger Receptor ACKR3/CXCR7, ACS Pharm. Transl. Sci. 4 (2021) 813–823, https://doi.org/10.1021/ACSPTSCI.1C00006/SUPPL_FILE/PT1C00006_SI_001.PDF.
[33] P.A. Longo, J.M. Kavran, M.-S. Kim, D.J. Leahy, Transient mammalian cell transfection with polyethylenimine (PEI), Methods Enzym. 529 (2013) 227–240, https://doi.org/10.1016/B978-0-12-418687-3.00018-5.
[34] F. Ciruela, M.M. Soloviev, W.-Y. Chan, R.A.J. McIlhinney, Homer-1c/Vesl-1L modulates the cell surface targeting of metabotropic glutamate receptor type 1α: Evidence for an anchoring function, Mol. Cell Neurosci. 15 (2000), https://doi.org/10.1006/mcne.1999.0808.
[35] X. Morató, D.O. Borroto-Escuela, K. Fuxe, V. Fernández-Dueñas, F. Ciruela, Co-immunoprecipitation from brain, Neuromethods 110 (2016) 19–30.
[36] V. Fernández-Dueñas, M. Qian, J. Argerich, C. Amaral, M.D.P. Risseeuw, S. van Calenbergh, F. Ciruela, Design, Synthesis and Characterization of a New Series of Fluorescent Metabotropic Glutamate Receptor Type 5 Negative Allosteric Modulators, Molecules 25 (2020), https://doi.org/10.3390/MOLECULES25071532.
[37] C. Laschet, N. Dupuis, J. Hanson, A dynamic and screening-compatible nanoluciferase-based complementation assay enables profiling of individual GPCR-G protein interactions, J. Biol. Chem. 294 (2019) 4079–4090, https://doi.org/10.1074/JBC.RA118.006231.
[38] J. Taura, V. Fernández-Dueñas, F. Ciruela, Determination of GPCR-mediated cAMP accumulation in rat striatal synaptosomes, Neuromethods 110 (2016) 455–464.
[39] A. Glukhova, D.M. Thal, A.T. Nguyen, E.A. Vecchio, M. Jörg, P.J. Scammells, L. T. May, P.M. Sexton, A. Christopoulos, Structure of the Adenosine A1 Receptor Reveals the Basis for Subtype Selectivity, e13, Cell 168 (2017) 867–877, https://doi.org/10.1016/j.cell.2017.01.042.
[40] E. Segala, D. Guo, R.K.Y. Cheng, A. Bortolato, F. Deflorian, A.S. Doré, J.C. Errey, L. H. Heitman, A.P. Ijzerman, F.H. Marshall, R.M. Cooke, Controlling the Dissociation of Ligands from the Adenosine A2A Receptor through Modulation of Salt Bridge Strength, J. Med Chem. 59 (2016) 6470–6479, https://doi.org/10.1021/ACS.JMEDCHEM.6B00653.
[41] S. Granier, A. Manglik, A.C. Kruse, T.S. Kobilka, F.S. Thian, W.I. Weis, B.K. Kobilka, Structure of the δ-opioid receptor bound to naltrindole, Nature 485 (2012) 400–404, https://doi.org/http://www.nature.com/nature/journal/v485/n7398/abs/nature11111.html#supplementary-information.
[42] G. Navarro, A. Cordomí, M. Zelman-Femiak, M. Brugarolas, E. Moreno, D. Aguinaga, L. Perez-Benito, A. Cortés, V. Casadó, J. Mallol, E.I. Canela, C. Lluís, L. Pardo, A.J. García-Sáez, P.J. McCormick, R. Franco, Quaternary structure of a G-protein-coupled receptor heterotetramer in complex with Gi and Gs, BMC Biol. 14 (2016) 26, https://doi.org/10.1186/s12915-016-0247-4.
[43] S. Schott-Verdugo, H. Gohlke, PACKMOL-Memgen, A simple-to-use, generalized workflow for membrane-protein-lipid-bilayer system building, J. Chem. Inf. Model 59 (2019), https://doi.org/10.1021/ACS.JCIM.9B00269.
[44] M.J. Abraham, T. Murtola, R. Schulz, S. Pall, J.C. Smith, B. Hess, E. Lindahl, GROMACS: high performance molecular simulations through multi-level parallelism from laptops to supercomputers, SoftwareX 1 2 (2015) 19–25.
[45] G. Navarro, A. Gonzalez, S. Campanacci, R. Rivas-Santisteban, I. Reyes-Resina, N. Casajuana-Martin, A. Cordomí, L. Pardo, R. Franco, Experimental and computational analysis of biased agonism on full-length and a C-terminally truncated adenosine A 2A receptor, Comput. Struct. Biotechnol. J. 18 (2020) 2723–2732, https://doi.org/10.1016/J.CSBJ.2020.09.028.
[46] N. Michaud-Agrawal, E.J. Denning, T.B. Woolf, O. Beckstein, MDAnalysis: a toolkit for the analysis of molecular dynamics simulations, J. Comput. Chem. 32 (2011) 2319–2327, https://doi.org/10.1002/JCC.21787.
[47] H.J. Motulsky, R.E. Brown, Detecting outliers when fitting data with nonlinear regression - A new method based on robust nonlinear regression and the false discovery rate, BMC Bioinforma. 7 (2006), https://doi.org/10.1186/1471-2105-7-123.
[48] A.S. Hauser, A.J. Kooistra, C. Munk, F.M. Heydenreich, D.B. Veprintsev, M. Bouvier, M.M. Babu, D.E. Gloriam, GPCR activation mechanisms across classes and macro/microscales, Nat. Struct. Mol. Biol. 28 (2021) 879–888, https://doi.org/10.1038/S41594-021-00674-7.
[49] W. Jespers, A.C. Schiedel, L.H. Heitman, R.M. Cooke, L. Kleene, G.J.P. van Westen, D.E. Gloriam, C.E. Müller, E. Sotelo, H. Gutiérrez-de-Terán, Structural Mapping of Adenosine Receptor Mutations: Ligand Binding and Signaling Mechanisms, Trends Pharm. Sci. 39 (2018) 75–89, https://doi.org/10.1016/j.tips.2017.11.001.
[50] W.I. Weis, B.K. Kobilka, The Molecular Basis of G Protein-Coupled Receptor Activation, Annu Rev. Biochem 87 (2018) 897–919, https://doi.org/10.1146/ANNUREV-BIOCHEM-060614-033910.
[51] J.R. Savinainen, S.M. Saario, R. Niemi, T. Järvinen, J.T. Laitinen, An optimized approach to study endocannabinoid signaling: evidence against constitutive activity of rat brain adenosine A1 and cannabinoid CB1 receptors, Br. J. Pharm. 140 (2003) 1451–1459, https://doi.org/10.1038/SJ.BJP.0705577.
[52] P. Högel, A. Götz, F. Kuhne, M. Ebert, W. Stelzer, K.D. Rand, C. Scharnagl, D. Langosch, Glycine Perturbs Local and Global Conformational Flexibility of a Transmembrane Helix, Biochemistry 57 (2018) 1326–1337, https://doi.org/10.1021/ACS.BIOCHEM.7B01197.
[53] X. Deupi, M. Olivella, C. Govaerts, J.A. Ballesteros, M. Campillo, L. Pardo, Ser and Thr residues modulate the conformation of pro-kinked transmembrane alpha-helices, Biophys. J. 86 (2004) 105–115, https://doi.org/10.1016/S0006-3495(04)74088-6.
[54] X. Deupi, M. Olivella, A. Sanz, N. Dölker, M. Campillo, L. Pardo, Influence of the g-conformation of Ser and Thr on the structure of transmembrane helices, J. Struct. Biol. 169 (2010) 116–123, https://doi.org/10.1016/J.JSB.2009.09.009.
[55] X. Wang, W. Jespers, K.A.N. Wolff, J. Buytelaar, A.P. IJzerman, G.J.P. van Westen, L.H. Heitman, Cancer-Related Somatic Mutations in Transmembrane Helices Alter Adenosine A1 Receptor Pharmacology, Molecules 27 (2022) 3742, https://doi.org/10.3390/MOLECULES27123742.
[56] L. Pardo, X. Deupi, N. Dölker, M.L. López-Rodríguez, M. Campillo, The role of internal water molecules in the structure and function of the rhodopsin family of G protein-coupled receptors, Chembiochem 8 (2007) 19–24, https://doi.org/10.1002/CBIC.200600429.
[57] C. Llinas Del Torrent, N. Casajuana-Martin, L. Pardo, G. Tresadern, L. Pérez-Benito, Mechanisms Underlying Allosteric Molecular Switches of Metabotropic Glutamate Receptor 5, J. Chem. Inf. Model 59 (2019) 2456–2466, https://doi.org/10.1021/ACS.JCIM.8B00924.
[58] A.J. Venkatakrishnan, A.K. Ma, R. Fonseca, N.R. Latorraca, B. Kelly, R.M. Betz, C. Asawa, B.K. Kobilka, R.O. Dror, Diverse GPCRs exhibit conserved water networks for stabilization and activation, Proc. Natl. Acad. Sci. USA 116 (2019) 3288–3293, https://doi.org/10.1073/PNAS.1809251116.
[59] G. Navarro, A. Cordomí, M. Brugarolas, E. Moreno, D. Aguinaga, L. Pérez-Benito, S. Ferre, A. Cortés, V. Casadó, J. Mallol, E.I. Canela, C. Lluís, L. Pardo, P. J. McCormick, R. Franco, Cross-communication between G i and G s in a G-protein-coupled receptor heterotetramer guided by a receptor C-terminal domain, BMC Biol. 16 (2018), https://doi.org/10.1186/S12915-018-0491-X.
[60] R. Franco, A. Cordomí, C. Llinas del Torrent, A. Lillo, J. Serrano-Marín, G. Navarro, L. Pardo, Structure and function of adenosine receptor heteromers, Cell Mol. Life Sci. 78 (2021) 3957–3968, https://doi.org/10.1007/S00018-021-03761-6.
[61] T. Schöneberg, I. Liebscher, Mutations in G protein-coupled receptors: mechanisms, pathophysiology and potential therapeutic approaches, Pharm. Rev. 73 (2021) 89–119, https://doi.org/10.1124/PHARMREV.120.000011.
[62] A.J. Kooistra, S. Mordalski, G. Pándy-Szekeres, M. Esguerra, A. Mamyrbekov, C. Munk, G.M. Keserű, D.E. Gloriam, GPCRdb in 2021: integrating GPCR sequence, structure and function, Nucleic Acids Res 49 (2021) D335–D343, https://doi.org/10.1093/NAR/GKAA1080.
[63] M.S. Rodrigues, S.G. Ferreira, C. Quiroz, C.J. Earley, D. García-Borreguero, R. A. Cunha, F. Ciruela, A. Köfalvi, S. Ferré, Brain iron deficiency changes the stoichiometry of adenosine receptor subtypes in cortico-striatal terminals: implications for restless legs syndrome, Molecules 27 (2022), https://doi.org/10.3390/MOLECULES27051489.
[64] S. Ferré, C. Quiroz, W. Rea, X. Guitart, D. García-Borreguero, Adenosine mechanisms and hypersensitive corticostriatal terminals in restless legs syndrome,

Ration. Use Inhib. Aden Transp., Adv. Pharm. 84 (2019) 3–19, https://doi.org/10.1016/BS.APHA.2018.12.005.

[65] F. Ciruela, C. Albergaria, A. Soriano, L. Cuffi, L. Carbonell, S. Sanchez, J. Gandia, V. Fernandez-Duenas, Adenosine receptors interacting proteins (ARIPs): Behind the biology of adenosine signaling, Biochim Biophys. Acta 2010 (1798) 9–20, https://doi.org/10.1016/j.bbamem.2009.10.016.

[66] C.J. Draper-Joyce, M. Khoshouei, D.M. Thal, Y.L. Liang, A.T.N. Nguyen, S.G. B. Furness, H. Venugopal, J.A. Baltos, J.M. Plitzko, R. Danev, W. Baumeister, L. T. May, D. Wootten, P.M. Sexton, A. Glukhova, A. Christopoulos, Structure of the adenosine-bound human adenosine A1 receptor-Gi complex, Nature 558 (2018) 559–565, https://doi.org/10.1038/s41586-018-0236-6.

[67] F. Ciruela, V. Casado, J. Mallol, E.I. Canela, C. Lluis, R. Franco, Immunological identification of A1 adenosine receptors in brain cortex, J. Neurosci. Res 42 (1995) 818–828, https://doi.org/10.1002/jnr.490420610.

[68] C.J. Tsai, F. Pamula, R. Nehmé, J. Mühle, T. Weinert, T. Flock, P. Nogly, P. C. Edwards, B. Carpenter, T. Gruhl, P. Ma, X. Deupi, J. Standfuss, C.G. Tate, G.F. X. Schertler, Crystal structure of rhodopsin in complex with a mini-G o sheds light on the principles of G protein selectivity, Sci. Adv. 4 (2018), https://doi.org/10.1126/SCIADV.AAT7052.

[69] M.A. Lomize, A.L. Lomize, I.D. Pogozheva, H.I. Mosberg, OPM: orientations of proteins in membranes database, Bioinformatics 22 (2006) 623–625, https://doi.org/10.1093/bioinformatics/btk023.